Amyloid-β fibrils assembled on ganglioside-enriched membranes contain both parallel β-sheets and turns

Received for publication, March 9, 2018, and in revised form, July 11, 2018 Published, Papers in Press, July 17, 2018, DOI 10.1074/jbc.RA118.002787

Teruhiko Matsubara[‡], Hanaki Yasumori[‡], Koichiro Ito[‡], Takafumi Shimoaka[§], Takeshi Hasegawa[§], and Toshinori Sato[‡1]

From the [‡]Department of Biosciences and Informatics, Keio University, 3-14-1 Hiyoshi, Kouhoku-ku, Yokohama 223-8522, Japan and the [§]Institute for Chemical Research, Kyoto University, Uji, Kyoto 611-0011, Japan

Edited by Paul E. Fraser

Some protein and peptide aggregates, such as those of amyloid-β protein (Aβ), are neurotoxic and have been implicated in several neurodegenerative diseases. Aβ accumulates at nanoclusters enriched in neuronal lipids called gangliosides in the presynaptic neuronal membrane, and the resulting oligomeric and/or fibrous forms accelerate the development of Alzheimer's disease. Although the presence of Aβ deposits at such nanoclusters is known, the mechanism of their assembly and the relationship between Aβ secondary structure and topography are still unclear. Here, we first confirmed by atomic force microscopy that $Aβ_{40}$ fibrils can be obtained by incubating seed-free $Aβ_{40}$ monomers with a membrane composed of sphingomyelin, cholesterol, and the ganglioside GM1. Using Fourier transform infrared (FTIR) reflection–absorption spectroscopy, we then found that these lipid-associated fibrils contained parallel β-sheets, whereas self-assembled $Aβ_{40}$ molecules formed antiparallel β-sheets. We also found that the fibrils obtained at GM1-rich nanoclusters were generated from turn $Aβ_{40}$. Our findings indicate that Aβ generally self-assembles into antiparallel β-structures but can also form protofibrils with parallel β-sheets by interacting with ganglioside-bound Aβ. We concluded that by promoting the formation of parallel β-sheets, highly ganglioside-enriched nanoclusters help accelerate the elongation of Aβ fibrils. These results advance our understanding of ganglioside-induced Aβ fibril formation in neuronal membranes and may help inform the development of additional therapies for Alzheimer's disease.

Protein and peptide aggregates are neurotoxic and are thus implicated in neurodegenerative diseases (1–3). In particular, amyloid precursor protein is digested by secretases to generate amyloid-β protein (Aβ),[2] a 39–43–residue polypeptide that oligomerizes and forms fibrils, which then accelerate the development of Alzheimer's disease (4–6). Oligomers and fibrils are often reported to contain β-sheets, based on CD (7) and solid-state nuclear magnetic resonance (NMR) (8–10). However, fibrillar Aβ with parallel β-sheets is distinct from oligomeric Aβ with antiparallel β-sheets, as assessed by solid-state NMR (11, 12) and Fourier transform infrared (FTIR) spectroscopy (13, 14).

Oligomerization and fibril formation are generally spontaneous (15) but are enhanced by numerous factors including metal ions (16, 17) and gangliosides (18). The latter, which abundant in the nervous system, are often visualized by cholera toxin B subunit, which binds GM1, Galβ1–3GalNAcβ1–4(Neu5Acα2–3)Galβ1–4Glc1–1′-Cer (19, 20). Levels of gangliosides including GM1 are within 1–2% in the extracellular leaflet of the plasma membrane in the nervous system (21). However, gangliosides actually exist with high density in lipid rafts comprising sphingomyelin and cholesterol (22). Ganglioside-enriched microdomains at neuronal membranes are considered among the key sites for the onset of Alzheimer's disease. Aβ assembly at neuronal membranes (23, 24), in which a ganglioside-bound Aβ (GAβ) complex acts as an endogenous seed, was first reported by Yanagisawa *et al.* (18) and was eventually demonstrated on ganglioside-containing liposomes using a thioflavin T assay, EM, and antibody assays (25, 26). The toxicity of the Aβ assembly resulting from the GAβ complex has been assessed using rat PC12 pheochromocytoma cells (27) and human neuroblastoma SH-SY5Y cells (28). These cells express gangliosides, including GM1, and nerve growth factor receptor–mediated neuronal cell death or cellular damage has been indicated. More recently, atomic force microscopy (AFM) of a reconstituted lipid bilayer containing mouse synaptosomal lipids has suggested that Aβ-sensitive ganglioside nanoclusters promote $Aβ_{40}$ assembly (29, 30). In addition, the chain length of ganglioside GD1b was found to influence $Aβ_{42}$ assembly at the neuronal membrane in human precuneus with amyloids (31).

Structural studies of Aβ polymerized at ganglioside-containing membranes are limited and contradictory. For example, Matsuzaki and Horikiri (32) found by CD that $Aβ_{40}$ forms β-sheets at liposomes containing GM1, *e.g.* liposomes of sphingomyelin/cholesterol/GM1 (5:2:3). Similarly, FTIR attenuated total reflection spectroscopy indicated that $Aβ_{40}$ forms antiparallel β-sheets at dry-cast films of egg yolk L-α-phosphatidylcholine/GM1/$Aβ_{40}$ (40:10:1) (32) or at liposomes of GM1/cho-

This work was supported by Kakenhi Grant 22300118 from the Japan Society for the Promotion of Science (to T. M.), by Grant 11-093 from the Suzuken Memorial Foundation (to T. M.), by the Keio Gijuku Academic Development Funds (to T. M.), and by Research Funding for Longevity Sciences, Grant 25-19, from the National Center for Geriatrics and Gerontology, Japan (to T. M.). The authors declare that they have no conflicts of interest with the contents of this article.

This article contains Figs. S1 and S2 and Table S1.

[1] To whom correspondence should be addressed. Tel.: 81-45-566-1771; E-mail: sato@bio.keio.ac.jp.

[2] The abbreviations used are: Aβ, amyloid-β protein; AFM, atomic force microscopy; GAβ, ganglioside-bound Aβ; GlcCer, glucosylceramide; POPC, 1-palmitoyl-2-oleoyl-*sn*-glycelo-3-phosphocholine; mN, millinewton.

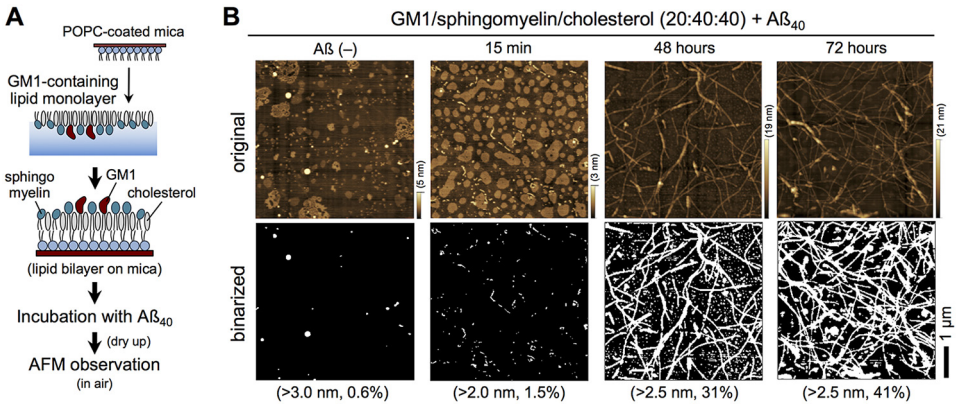

Figure 1. Formation of Aβ fibrils on GM1-enriched membranes. *A*, preparation of GM1-enriched membranes for AFM. A monolayer of GM1/sphingomyelin/cholesterol (20:40:40) was deposited on POPC-coated mica to form a bilayer. *B*, AFM images of GM1/sphingomyelin/cholesterol (20:40:40) membranes after incubation with 10 μM Aβ_{40} at 37 °C for 0 min (Aβ(−)), 15 min, 48 h, and 72 h (*upper panel*). Heights are indicated by *color bars*. Binarized AFM images were obtained by thresholding at 2.0–3.0 nm from the bottom, and percentages represent the total area higher than the indicated height (*lower panel*). *Scale bar*, 1 μm.

lesterol/sphingomyelin (4:3:3) (33). On the other hand, NMR data collected by Utsumi *et al.* (34–36) suggest that Aβ_{40} forms α-helices at membranes containing GM1 because of the hydrophobic environment. Recently, Hu *et al.* (37) also showed by Raman spectroscopy that α-helices and β-sheets of Aβ_{40} were eventually observed with a planar lipid bilayer composed of GM1/sphingomyelin/cholesterol (5:55:40 and 20:40:40), although the topography of the fibrils was not investigated. Among these studies, spectroscopic evidence of ganglioside-induced fibrillar Aβ with parallel β-sheets has not yet been reported. In light of these results, a unifying model of Aβ assembly is needed to explain most of the structural data.

Previously, we found that Aβ-sensitive ganglioside nanoclusters in neuronal membranes induce a conformational change in Aβ_{40} (29, 38). This and other characteristic properties of Aβ-sensitive ganglioside nanoclusters are mimicked by ganglioside-enriched planar membranes composed of ganglioside (GM1, GM2, GD1a, GD1b, or GT1b)/sphingomyelin/cholesterol (10:45:45) (30). These membranes are constructed by depositing a monolayer composed of ganglioside, sphingomyelin, and cholesterol with a lateral plasma membrane pressure (30 mN m^{-1}) on phospholipid-coated mica. This type of membrane is more stable than conventional liposomes (39) and supported lipid bilayers (37) with the same lipid composition, and AFM images can be obtained in a few days. In addition, various lipid compositions of the membrane are acceptable even if there are lipids incapable of forming liposomes.

Using FTIR reflection–absorption spectroscopy, we have now determined the secondary structure of Aβ_{40} fibrils obtained in 15 min to 72 h on membranes containing GM1 at a 20% molar ratio (GM1/sphingomyelin/cholesterol, 20:40:40). The data indicate that the fibrils form turns and parallel β-sheets within 48 h. On the other hand, Aβ_{40} assembled on membranes with 20% glucosylceramide (GlcCer), as well as self-assembled Aβ_{40}, forms antiparallel β-sheets. Solid-state NMR analyses by Tycko and co-workers (10, 40, 41) indicate that Aβ_{40} predominantly forms cross–β-structures based on parallel β-sheets stabilized by intermolecular hydrogen bonds. Our results imply that by promoting the formation of parallel β-sheets, highly ganglioside-enriched nanoclusters also accelerate the elongation of Aβ fibrils.

Results

Formation of Aβ fibrils on GM1-enriched membranes

As described previously (30), Aβ_{40} fibrils were formed at ganglioside-enriched, planar, bilayer membranes, which were prepared by depositing 20:40:40 monolayers of GM1, sphingomyelin, and cholesterol onto 1-palmitoyl-2-oleoyl-*sn*-glycelo-3-phosphocholine (POPC)– coated mica (GM1-enriched membrane (Fig. 1*A*)). This composition mimics that of GM1-enriched microdomains and has frequently been used for ganglioside-induced Aβ assembly (39, 42). To confirm fibril formation, membranes were imaged by AFM in water after incubation with Aβ_{40}. GM1-enriched microdomains and Aβ assemblies were then visualized as areas higher than 4 nm on binarized AFM images. GM1-enriched microdomains before incubation with Aβ_{40} had a diameter of 30–300 nm (>700 domains in a 5 μm × 5 μm area), and the apparent size of the domains increased after incubation with Aβ_{40} for 15 min (60–500 nm, 280 domains) (Fig. S1). This topological change suggests that Aβ molecules are deposited on the GM1-enriched membrane to yield an Aβ layer (30). After 48 h, over a dozen Aβ_{40} fibrils >1-μm long were clearly observed in a 5 × 5-μm area. These Aβ fibrils accumulated on round-shaped GM1-enriched microdomains, as reported previously (30).

To measure FTIR in air, after the formation of Aβ_{40} fibrils, membranes were dried overnight and imaged in air (Fig. 1*B*, *upper panel*). The binalized AFM images of GM1-enriched membranes after incubation with Aβ_{40} for 15 min, 48 h, and 72 h are shown in Fig. 1*B* (*lower panel*) at a height threshold of 2.0–3.0 nm. Drying slightly altered the shape of GM1-enriched microdomains, but Aβ_{40} fibrils were still identifiable, and more Aβ_{40} fibrils were observed after 72 h than after 48 h. On the other hand, one long fibril (>3 μm) and several short fibrils were observed on GlcCer-enriched membranes after 72 h (Fig. 2). These results indicate that GM1 generates and elongates Aβ fibrils more effectively than GlcCer.

Immobilization of GM1-enriched membranes on gold-coated glass

FTIR reflection–absorption spectra were collected to investigate the formation of lipid bilayers on gold-coated glass. Seven characteristic peaks in a monolayer of POPC were assigned according to the literature to CH_3, CH_2, PO_2^-, and ester C–O stretching vibration (Fig. 3*A* and Table 1) (43, 44). A strong peak corresponding to C=O stretching vibration (ν(C=O), 1742 cm^{-1}) was also observed. On the other hand, amide I (1660 cm^{-1}) and amide II (1547 cm^{-1}) were observed in monolayers containing GM1 or GlcCer at a 20% molar ratio, as both lipids contain ceramide (44, 45). Two peaks, at 3342 and 1379 cm^{-1}, in these membranes were assigned to N–H stretching and $-CH_3$ scissoring vibration, respectively. The spectrum of a lipid bilayer composed of POPC as the first layer and GM1/sphingomyelin/cholesterol as the second layer is simply a superposition of the spectrum of each, clearly implying that a lipid bilayer with GM1 was formed on gold-coated glass.

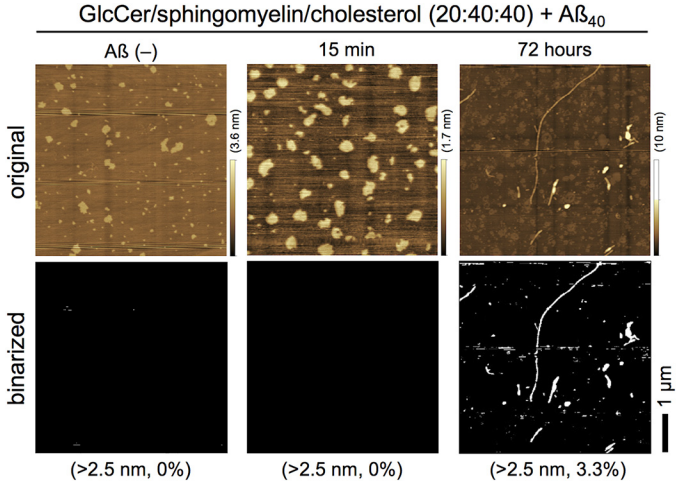

Figure 2. Formation of Aβ fibrils on GlcCer-enriched membranes. *Upper panel*, AFM images of GlcCer/sphingomyelin/cholesterol (20:40:40) membranes after incubation with 10 μM $A\beta_{40}$ at 37 °C for 0 min (Aβ(−)), 15 min, and 72 h. Heights are indicated by *color bars*. *Lower panel*, binarized AFM images were obtained via thresholding at 2.5 nm from the bottom, and percentages represent the total area higher than the indicated height. *Scale bar*, 1 μm.

Aβ deposition on GM1- and GlcCer-enriched membranes

To investigate the interaction between Aβ and a GM1-enriched membrane, FTIR reflection–absorption spectra were collected after 15 min, 24 h, 48 h, and 72 h. Incubation with $A\beta_{40}$ shifted amide I and II peaks to 1663 and 1541 cm^{-1}, respectively (Fig. 3*B*, *upper panel*, and Table S1). In addition, the height of these peaks significantly increased with time, as plotted in Fig. 4 along with peak shifts, indicating $A\beta_{40}$ accumulation. The absorbance continued to increase even at 72 h, although peak shifts had nearly stabilized by that point.

The amide I and II bands in GlcCer-enriched membranes were at positions similar to those in GM1-enriched membranes (Fig. 3*B*, *lower panel*, and Fig. 4), implying comparable molecular structures in both membranes in light of the surface selection rule of reflection–absorption spectroscopy. In addition, the peaks were of similar relative intensity at 15 min and 72 h, implying comparable $A\beta_{40}$ accumulation on both membranes, despite drastic differences in their ability to form fibrils (Figs. 1*B* and 2).

Secondary structure of Aβ fibrils based on second-derivative reflection–absorption spectra

The secondary structure of $A\beta_{40}$ fibrils deposited on GM1-enriched membranes was determined from the reflection–absorption spectra of amide I (1700–1600 cm^{-1}) region and the corresponding second-derivative reflection spectra (46–49). The antiparallel β-sheet (pair of peaks, 1612–1640 and 1670–1690 cm^{-1}), parallel β-sheet (1626–1640 cm^{-1}), and turn structures (1655–1675 cm^{-1} and/or 1680–1696 cm^{-1}) were determined on the basis of previous reports (50, 51).

The strongest peak of the amide I region from 15 min to 72 h was shifted from 1676 to 1663 cm^{-1} observed in the raw spectrum of GM1-enriched membranes (Fig. 3*B*, *upper panel*, Fig. S2, and Table S1). The second-derivative reflection spectra indicated that two peaks (1661–1662 and 1691–1695 cm^{-1})

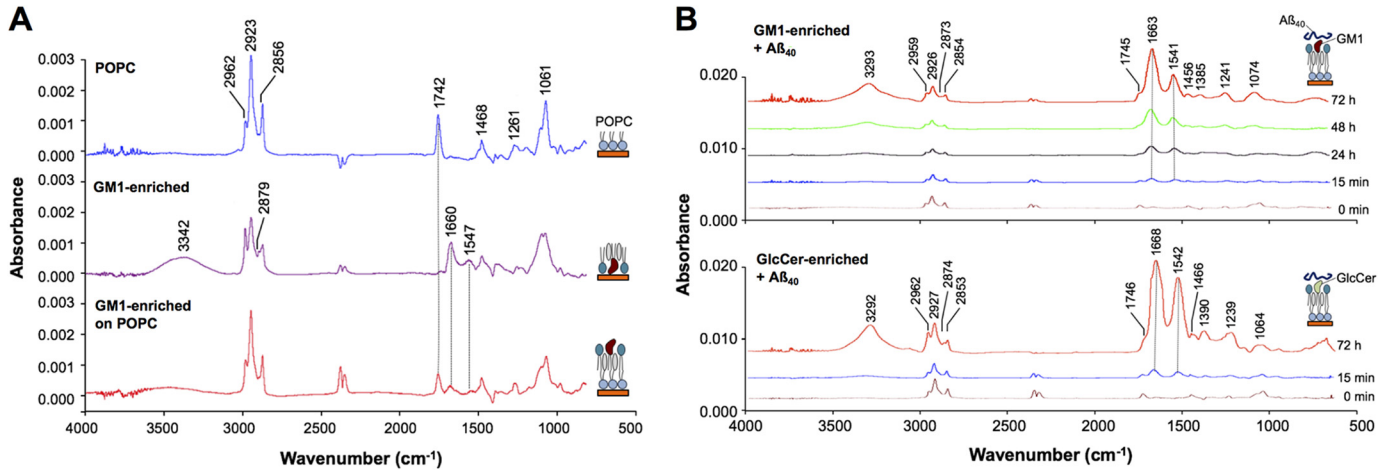

Figure 3. FTIR reflection–absorption spectra of GM1-enriched membrane. *A*, a POPC monolayer (*top*), a GM1/sphingomyelin/cholesterol (20:40:40) monolayer (*middle*), and a bilayer of POPC and GM1/sphingomyelin/cholesterol (20:40:40) (*bottom*). Peak assignments are listed in Table 1. *B*, GM1/sphingomyelin/cholesterol (20:40:40) (*upper panel*) and GlcCer/sphingomyelin/cholesterol (20:40:40) (*lower panel*) membranes after incubation with $A\beta_{40}$ for 0 min to 72 h. Amide I and amide II are around 1663–1668 and 1541–1542 cm^{-1}, respectively. Peak assignments are listed in Table S1.

Table 1
Peak assignment in reflection–absorption spectra

Lipid layer (wavenumber)						
POPC	GM1[a]	GlcCer[b]	POPC + GM1[a]	POPC + GlcCer[b]	Assignment	Ref. No.
		cm^{-1}				
	3342	3331			O–H, N–H stretching	(43)
2962	2964	2963	2961	2961	Asymmetric stretching $-CH_3$	(43, 44)
2923	2927	2926	2927	2927	Asymmetric stretching $-CH_2-$	(43, 44)
2880	2879	2879	2879	2879	Symmetric stretching $-CH_3$	(43)
2856	2855	2855	2856	2856	Symmetric stretching $-CH_2-$	(43, 44)
1742		1731	1741	1742	C=O stretching	(44)
	1660	1664	1667	1667	Amide I	(44, 45)
	1547	1541			Amide II	(44, 45)
1468	1466	1468	1468	1469	Scissoring bending $-CH_2-$	(43, 44)
	1379	1379	1379	1376	Scissoring bending $-CH_3$	(43, 44, 45)
1261	1243	1244	1251	1251	PO_2^- asymmetric stretching	(44)
1061	1065	1060	1058	1058	PO_2^- symmetric, C–O stretching	(44)

[a] GM1/sphingomyelin/cholesterol (20:40:40).
[b] GlcCer/sphingomyelin/cholesterol (20:40:40).

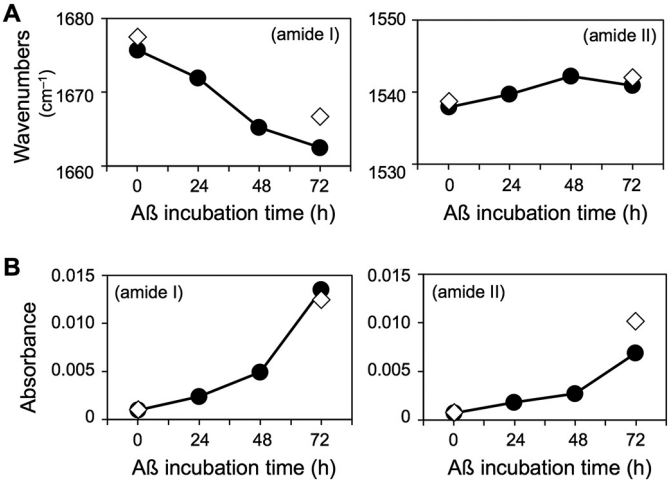

Figure 4. Time-dependent changes in amide I and II peaks in GM1/sphingomyelin/cholesterol (20:40:40) (*closed circles*) and GlcCer/sphingomyelin/cholesterol (20:40:40) (*open diamonds*) membranes incubated with $A\beta_{40}$. Shifts in wavenumber (*A*) and changes in intensity (*B*) were observed.

corresponding to the turns were appeared after 48 and 72 h (Fig. 5*A*, Table 1, and Fig. S2).

On the other hand, a strong peak at 1668 cm^{-1} with two shoulders was observed in the raw spectrum of GlcCer-enriched membranes after 72 h (Figs. 3*B*, *lower panel*, and 5*B*). The second-derivative spectra indicate that the two shoulders segregate into two peaks at 1631 and 1697 cm^{-1}. Because the peak of GlcCer-enriched membranes after 72 h at 1631 cm^{-1} was distinguishable from that of GM1-enriched membranes at 1635 cm^{-1}, these peaks at 1631 and 1635 cm^{-1} are assigned to antiparallel and parallel β-sheets, respectively (51). Two peaks, at 1631 and 1676 cm^{-1}, of GlcCer-enriched membranes were assigned to a pair of peaks for antiparallel β-sheets. From these results, we concluded that GM1-enriched membranes induced $A\beta_{40}$ fibrils with parallel β-sheets, in contrast to GlcCer-enriched membranes with antiparallel β-sheets (Fig. 5*C* and Table 2).

Secondary structure of self-assembled Aβ based on attenuated total reflection spectra

Seed-free $A\beta_{40}$ was self-assembled for 15 min and 48 h (6), dropped on a suitable plate, and dried under nitrogen gas for 50 min. Three peaks at around 1630, 1670, and 1697 cm^{-1} in the attenuated total reflection spectrum at 15 min were again observed in the spectrum at 48 h (Fig. 6*A*). The pair of peaks at 1630 and 1666–1670 cm^{-1} in the second-derivative spectra are characteristic of antiparallel β-sheets because the major component at 1612–1640 cm^{-1} was accompanied by a minor component at 1670–1690 cm^{-1} (Table 2) (50). The peak at 1697 cm^{-1} is attributed to a turn structure.

Structural features of residual Aβ in the supernatant incubated with GM1-enriched membranes

Although $A\beta_{40}$ fibrils formed on GM1-enriched membranes contain turns and parallel β-sheets (Fig. 5*A*), raw and second-derivative attenuated total reflection spectra (Fig. 6*B*) indicate that residual $A\beta_{40}$ in the supernatant is structurally similar to self-assembled $A\beta_{40}$, with major and minor components at 1630 and 1679 cm^{-1} corresponding to antiparallel β-sheets (Table 2). An AFM image of the residual $A\beta_{40}$ in the supernatant after a 48-h incubation with a GM1-enriched membrane supports the FTIR spectra, short fibrils, 150 nm or less in length, were observed (Fig. 6*C*).

Discussion

The objective of this study was to investigate the secondary structure of Aβ assembled on GM1-enriched membranes with a view to clarify the mechanism of assembly. Often, Aβ assembly on ganglioside-containing membranes is investigated in solution by fluorescence thioflavin T assay and CD, because such membranes are often prepared as liposomes. However, seemingly contradictory results have been reported, preventing the formulation of a unified mechanism of ganglioside-induced Aβ assembly. For example, Fukunaga *et al.* (33) reported that GM1-induced $A\beta_{40}$ contains antiparallel β-sheets based on FTIR but did not observe the α-helices detected on NMR (36). Recently, α-helices and β-sheets were detected by Raman spectroscopy of $A\beta_{40}$ deposited for 24 h on supported lipid bilayers composed of GM1/sphingomyelin/cholesterol (5:55:40 and 20:40:40) (37). There is no evidence of ganglioside-induced fibrillar $A\beta_{40}$ with parallel β-sheets that implies cross-β structures (10, 40, 41). Most unfortunately, however, the topography of Aβ assemblies are not always investigated when the secondary structure of Aβ assemblies is assessed.

We attempted to image $A\beta_{40}$ assemblies directly with time via AFM using membranes containing GM1/sphingomyelin/

cholesterol (20:40:40) on mica (29, 30). The images confirmed that $A\beta_{40}$ fibrils were formed on such membranes after 48–72 h but not on membranes containing GlcCer (Figs. 1*B* and 2). We have now determined from the secondary structures of $A\beta_{40}$ assemblies from second-derivative reflection–absorption spectra (Fig. 5*A*) that $A\beta_{40}$ fibrils deposited on GM1-enriched membranes for 48–72 h consist of turns (1661–1662 cm^{-1} and 1691–1695 cm^{-1}) and parallel β-sheets (1635–1637 cm^{-1}). The parallel β-sheets are clearly distinguishable from antiparallel β-sheets, typified by two characteristic peaks at 1631 and 1676 cm^{-1}, formed on GlcCer-enriched membranes (Fig. 5*B*). In this case, the difference in secondary structure correlates with the AFM data (Figs. 1 and 2).

In light of our results, a model of ganglioside-induced Aβ assembly was proposed (Fig. 7) in which monomeric Aβ forms an initial layer not only on GM1-enriched nanoclusters but also on sphingomyelin/cholesterol area (*step a*) (29, 30). NMR (36) and Raman spectroscopic studies (37) indicated that Aβ at ganglioside nanoclusters then forms helices (*step b*, GAβ formation); however, a prominent helical peak at 1650–1657 cm^{-1} was not observed (see Fig. 5*A*). Subsequently, Aβ molecules in contact with ganglioside-bound helical Aβ formed turn and antiparallel β-sheets and transited to parallel β-sheets (Fig. 7, *steps c* and *d*) (14). Previous FTIR findings of GM1-induced Aβ with antiparallel β-sheets, reported by Matsuzaki and Horikiri (32) and Fukunaga *et al.* (33), seem to resemble the present oligomeric Aβ assembly (Fig. 7, *steps c* and *f*). Finally, protofibrils with parallel β-sheets were formed and extended (Fig. 7, *step e*) as observed on reflection–absorption spectra at 48–72 h (Fig. 5*A*). The parallel β-sheet structure is stabilized by intermolecular interactions between Aβ molecules and β-sheet side chains to form cross-β units (9). Multiple molecular dynamics simulations support the binding of Aβ to ganglioside clusters through the combination of a CH–π/OH–π interaction, a Lys^{28}–Neu5Ac interaction, and hydrophobic interactions at the C terminus and also support the involvement of two or three Aβ molecules of the GAβ complex in the formation of the parallel β-sheet (52).

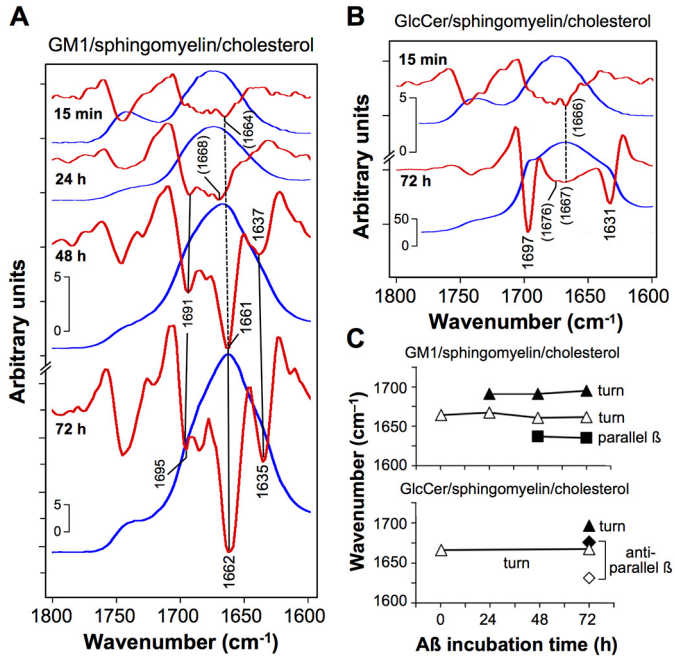

Figure 5. Time course of formation of $A\beta_{40}$ assemblies on GM1-enriched membranes. *A* and *B*, raw (*blue lines*) and second-derivative (*red lines*) reflection–absorption amide I spectra of $A\beta_{40}$ fibrils deposited for 15 min to 72 h on GM1/sphingomyelin/cholesterol (20:40:40) (*A*) and GlcCer/sphingomyelin/cholesterol (20:40:40) (*B*). The assigned peaks are summarized in *C*.

Table 2

Secondary structure assignment of amide I peaks in second-derivative reflection–absorption and attenuated total reflection (ATR) spectra of $A\beta_{40}$ assemblies

	20% GM1 on POPC					20% GlcCer on POPC		Self-assembled	
	15 min	24 h	48 h	72 h	48 h (ATR)	15 min	72 h	15 min (ATR)	48 h (ATR)
Assignment	Deposited	Oligomer/fibrils	Fibrils	Fibrils	Supernatant	Deposited	Oligomer/fibrils	Aggregates	Aggregates
Parallel β			1637	1635					
Antiparallel β					1630/1679		1631/1676[a]	1630/1666	1630/1670
Turn	1664[a]	1668[a]/1691	1661/1691	1662/1695	1695	1666[a]	1667[a]/1697	1697	1697

[a] Weak peaks.

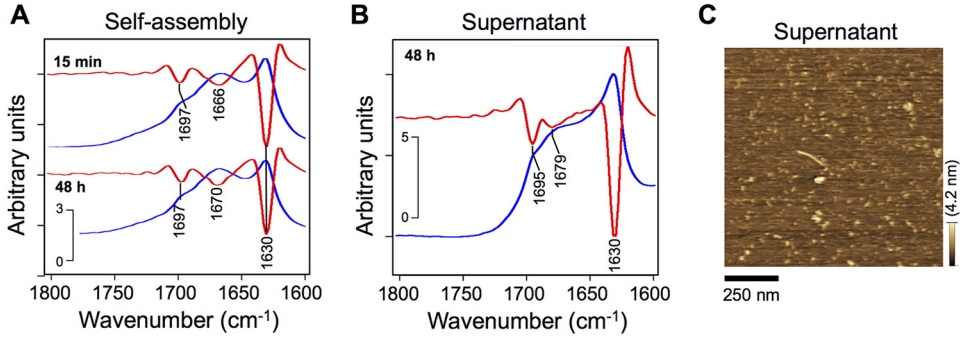

Figure 6. Formation of $A\beta_{40}$ assemblies in solution. *A* and *B*, raw (*blue lines*) and second-derivative (*red lines*) attenuated total reflection amide I spectra of self-assembled $A\beta_{40}$ (*A*) and residual $A\beta_{40}$ in the supernatant of solution on GM1-enriched membranes (*B*). After incubation at 25 °C for 15 min to 48 h, samples were dropped on a suitable plate and dried under nitrogen gas. *C*, an AFM image of residual $A\beta_{40}$ in the supernatant of solution after 48 h on GM1-enriched membranes. GM1/sphingomyelin/cholesterol (20:40:40) membrane was incubated with 10 μM $A\beta_{40}$ at 37 °C for 48 h, and thereafter the supernatant was dropped on a mica plate for 15 min. After washing, $A\beta_{40}$ deposited on the mica was imaged via AFM in water.

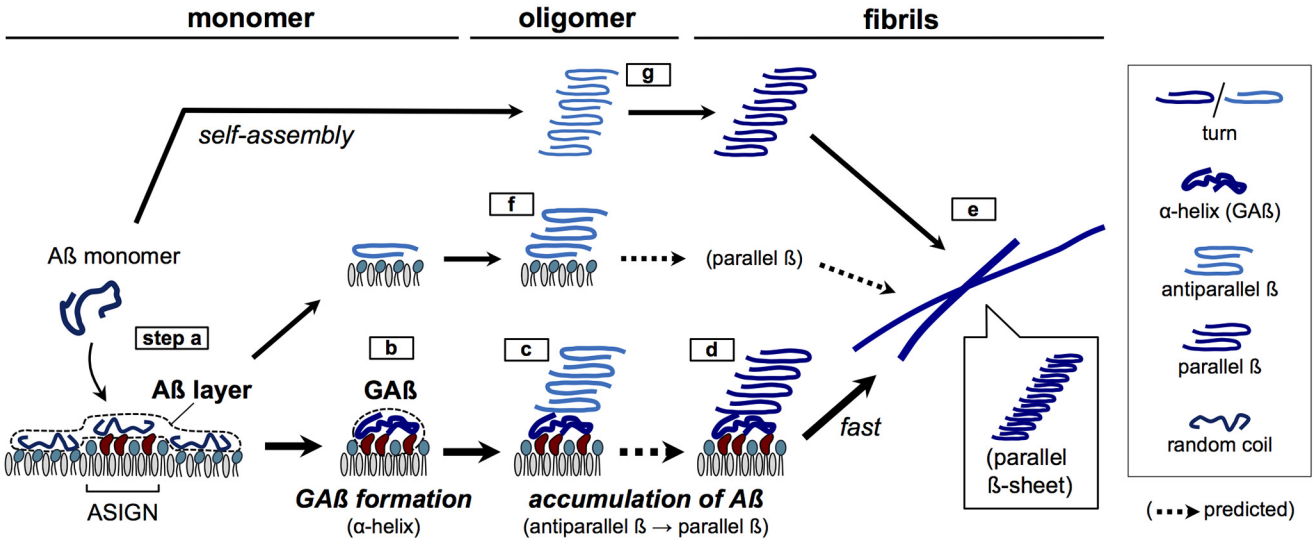

Figure 7. Proposed model of ganglioside-induced Aβ assembly in neural membranes, resulting in Alzheimer's disease. The formation of Aβ fibrils with parallel β-sheet on Aβ-sensitive ganglioside nanoclusters (*ASIGN*) (*a*–*e*) is faster than self-assembled oligomers with antiparallel β-sheet (*f* and *g*). *Steps d* and *e* are shown in Fig. 5*A*. *Steps f* and *g* are shown in Figs. 5*B* and 6*A*, respectively. *GAβ*, ganglioside-bound Aβ complex on ASIGN.

Based on attenuated total reflection spectra, the secondary structure of residual $A\beta_{40}$ in the supernatant of the solution on GM1-enriched membranes is similar to that of $A\beta_{40}$ deposited on GlcCer-rich membranes, with a major (1631 cm^{-1}) and a minor peak (1676 cm^{-1}) attributable to antiparallel β-sheets (Fig. 6*B*), which were also detected in $A\beta_{40}$ self-assembled for 48 h (Fig. 6*A*). Indeed, most of the residual $A\beta_{40}$ molecules in the supernatant may not interact at all with the GM1-enriched membrane and therefore will self-assemble in the same way as seed-free $A\beta_{40}$ (Fig. 6*C*). $A\beta_{40}$ self-oligomerized into antiparallel β-sheets (Fig. 7, *step g*), as described previously by Stroud *et al.* (13) and Fu *et al.* (14) and confirmed by reflection–absorption spectroscopy of self-assembled $A\beta_{40}$ and residual $A\beta_{40}$ in the supernatant of the solution on GM1-enriched membranes after 48 h (Fig. 6). That $A\beta_{40}$ deposited on GlcCer/sphingomyelin/cholesterol also formed antiparallel β-sheets (Fig. 5*B*), confirming that a GM1-enriched nanocluster is required to form fibrils with parallel β-sheets.

We noted that a mixture of GM1/sphingomyelin/cholesterol (20:40:40) formed a lipid bilayer with POPC on gold-coated glass as well as on mica (Fig. 1*A*) (30), with characteristic peaks of POPC (ν(C=O), 1742 cm^{-1}) and GM1 (amide I and II, 1660 and 1547 cm^{-1}, respectively) observable on reflection–absorption spectra (Fig. 3*A* and Table 1). The transfer ratio of the 20% GM1 monolayer onto the POPC-coated slide was almost 1.0 (see "Experimental Procedures"), implying the formation of a suitable bilayer of 20% GM1 and POPC. The intensity (absorbance) of amides I and II in GM1- and GlcCer-containing membranes increased with time (Fig. 3), suggesting an accumulation of Aβ. This result also suggests a comparable accumulation of an Aβ layer on both membranes, although AFM indicated that Aβ fibrils were selectively deposited on GM1-enriched membranes only (Figs. 1*B* and 2), as reported previously (30).

In conclusion, the data indicate that Aβ generally self-assembles into antiparallel β-structures but is competent to form protofibrils with parallel β-sheets, in this case by interaction with GAβ. This model is based on data from AFM and FTIR of a ganglioside-enriched planar membrane. The $A\beta_{40}$ topography obtained by AFM was eventually linked to secondary structures obtained by FTIR. In addition, an initial Aβ layer was also detected by both methods, suggesting that the formation of this layer may explain the seemingly contradictory data in the literature. Our data also highlight the growing significance of molecular dynamics simulation in investigating the interaction between Aβ and neural membranes. Finally, these data advance our understanding of ganglioside-induced Aβ fibril formation on neuronal membranes, which may accelerate the development of novel therapies against Alzheimer's disease.

Experimental procedures

Lipids

Monosialoganglioside GM1 from bovine brain and GlcCer from human (Gaucher disease) spleen were purchased from Sigma or Wako Pure Chemical Industries, Ltd. (Osaka, Japan). Sphingomyelin from bovine brain and synthetic POPC were from Matreya LLC (State College, PA) and Sigma, respectively.

Preparation of seed-free soluble $A\beta_{40}$

Seed-free soluble $A\beta_{40}$ was prepared as described previously (29, 30). In brief, synthetic Aβ (human, 1–40; code 4379-v, Peptide Institute Inc., Osaka, Japan) was dissolved in ice-cold 0.02% ammonia and ultracentrifuged at 560,000 × *g* for 3 h at 4 °C to remove undissolved peptide aggregates. The seed-free fraction (40–110 μM) was stored in aliquots at −80 °C until used. Prior to use, aliquots were diluted in Dulbecco's PBS(−), pH 7.4 (Nissui Pharmaceutical Co., Ltd., Tokyo, Japan).

Preparation of GM1-enriched membranes and AFM

GM1-enriched lipid bilayers were prepared on mica as described previously (29, 30). Briefly, a POPC monolayer was prepared at 25 °C at the air–water interface of a Langmuir–Blodgett trough (FSD-220, USI Corp., Fukuoka, Japan), with

water as the subphase, and deposited horizontally on freshly cut 1 × 1-cm mica at a surface pressure of 35 mN m^{-1} (Fig. 1*A*, POPC-coated mica). To form the bilayer, a second monolayer consisting of GM1/sphingomyelin/cholesterol (20:40:40, molar ratio) at a surface pressure of 30 mN m^{-1} was loaded horizontally onto POPC-coated mica by deposition.

The GM1-enriched membrane was incubated with 10 μM seed-free soluble Aβ_{40} in PBS for 15 min to 72 h at 37 °C (30, 31). After washing three times with PBS, the membrane was imaged at 25 °C in water using an SPM-9600 atomic force microscope (Shimadzu Corp., Kyoto, Japan) and a 38-μm soft cantilever (BL-AC40TS-C2, Olympus, Tokyo, Japan) with integrated pyramidal silicon nitride tips with spring constant 0.1 N m^{-1}. Multiple topographic images (2 × 2 μm, $n \geq 3$) were acquired in dynamic mode at 1–2 Hz, and representative images were used in further analyses.

To estimate the Aβ-coated areas, AFM images were binarized based on height, and pixels were counted using the GNU Image Manipulation Program. In particular, areas higher than around 4 nm on a binarized image were considered Aβ-coated layers. Fibril length and domain size were measured in ImageJ (National Institutes of Health, Bethesda, MD) using a line drawn along a fibril. We estimated the lengths of the long and short axes of an Aβ assembly and defined them as fibrils when the long/short axis aspect ratio was >3.

Immobilization of GM1-enriched membranes onto gold-coated glass

Glass slides (40 × 20 × 1.1 mm) coated with an evaporated gold layer 300 nm thick and a stabilizing chromium layer 50 nm thick were purchased from Geomatec (Yokohama, Japan) and treated for 10 min with a UV/ozone cleaner (Procleaner™ Plus, BioForce Nanosciences) to remove organic impurities. The slide was then coated by vertical deposition at a surface pressure of 35 mN m^{-1} with a POPC monolayer prepared at 25 °C at the air–water interface of a Langmuir minitrough (Minitrough System 2, KSV Instruments Ltd., Helsinki, Finland) with water as the subphase. After drying overnight, a monolayer consisting of GM1/sphingomyelin/cholesterol (20:40:40) or GlcCer/sphingomyelin/cholesterol (20:40:40) was deposited horizontally at a surface pressure of 30 mN m^{-1}. The transfer ratio of lipid to the slide was 1.0 ± 0.2 as calculated from changes in the lipid area and the area of the slide that thickened. Finally, the GM1-enriched lipid bilayer was incubated for 15 min to 72 h at 37 °C with 10 μM seed-free soluble Aβ_{40} in PBS. After careful washing with water three times, the membrane was dried overnight for FTIR reflection–absorption spectroscopy.

Reflection–absorption spectroscopy

IR spectra were recorded on a Magna 550 FTIR spectrometer (Thermo Fisher Scientific) equipped with a VR1-NIC variable-angle reflection accessory (Harrick Scientific Products, Inc., Pleasantville, NY) and an Hg-Cd-Te detector cooled with liquid nitrogen (53). A *p*-polarized IR ray was obtained using a wire grid polarizer (PWG-U1R, Harrick Scientific Products, Inc.). Data were collected at a modulation frequency 60 kHz, with angle of incidence 80° from the surface normal and number of accumulations 1000.

Attenuated total reflection spectroscopy

Attenuated total reflection spectra were collected as described previously (53). Briefly, 84 μM seed-free soluble Aβ_{40} in MilliQ water was incubated at 25 °C for 15 min or 48 h to induce self-assembly. About 15 μl of the resulting solution was dropped on a germanium plate and dried under nitrogen gas for 50 min. Spectra were collected using a single-reflection accessory (Spectra-Tech Foundation Performer, Thermo Fisher Scientific) and a germanium prism, with number of accumulations 1000. To compare these with the reflection–absorption spectra, attenuated total reflection spectra were transformed into absorbance (α) spectra according to $\alpha = 4\pi k/\lambda$, where k and λ are the imaginary parts of the complex refractive index (1.5) and the wavelength, respectively.

Second-derivative analysis of FTIR spectra

FTIR spectra were analyzed in OMNIC, version 7.3. The second derivative (54) of each spectrum was calculated by the Savitzky–Golay method (55).

Author contributions—T. M. conceptualization; T. M., H. Y., T. Shimoaka, and T. H. formal analysis; T. M. funding acquisition; T. M. and T. Sato investigation; T. M. writing-original draft; T. M. project administration; H. Y., K. I., and T. Shimoaka data curation; H. Y., T. Shimoaka, T. H., and T. Sato writing-review and editing; T. Shimoaka, T. H., and T. Sato resources; T. H. and T. Sato supervision.

References

1. Chiti, F., and Dobson, C. M. (2017) Protein misfolding, amyloid formation, and human disease: A summary of progress over the last decade. *Annu. Rev. Biochem.* **86,** 27–68 CrossRef Medline
2. Hardy, J., and Selkoe, D. J. (2002) The amyloid hypothesis of Alzheimer's disease: Progress and problems on the road to therapeutics. *Science* **297,** 353–356 CrossRef Medline
3. Sipe, J. D., and Cohen, A. S. (2000) Review: History of the amyloid fibril. *J. Struct. Biol.* **130,** 88–98 CrossRef Medline
4. Benzinger, T. L., Gregory, D. M., Burkoth, T. S., Miller-Auer, H., Lynn, D. G., Botto, R. E., and Meredith, S. C. (1998) Propagating structure of Alzheimer's beta-amyloid(10–35) is parallel beta-sheet with residues in exact register. *Proc. Natl. Acad. Sci. U.S.A.* **95,** 13407–13412 CrossRef Medline
5. Duff, K., Eckman, C., Zehr, C., Yu, X., Prada, C. M., Perez-tur, J., Hutton, M., Buee, L., Harigaya, Y., Yager, D., Morgan, D., Gordon, M. N., Holcomb, L., Refolo, L., Zenk, B., *et al.* (1996) Increased amyloid-beta42(43) in brains of mice expressing mutant presenilin 1. *Nature* **383,** 710–713 CrossRef Medline
6. Burdick, D., Soreghan, B., Kwon, M., Kosmoski, J., Knauer, M., Henschen, A., Yates, J., Cotman, C., and Glabe, C. (1992) Assembly and aggregation properties of synthetic Alzheimer's A4/beta amyloid peptide analogs. *J. Biol. Chem.* **267,** 546–554 Medline
7. McLaurin, J., and Chakrabartty, A. (1996) Membrane disruption by Alzheimer beta-amyloid peptides mediated through specific binding to either phospholipids or gangliosides: Implications for neurotoxicity. *J. Biol. Chem.* **271,** 26482–26489 CrossRef Medline
8. Lansbury, P. T., Jr., Costa, P. R., Griffiths, J. M., Simon, E. J., Auger, M., Halverson, K. J., Kocisko, D. A., Hendsch, Z. S., Ashburn, T. T., Spencer, R. G. *et al.* (1995) Structural model for the beta-amyloid fibril based on interstrand alignment of an antiparallel-sheet comprising a C-terminal peptide. *Nat. Struct. Biol.* **2,** 990–998 CrossRef Medline

9. Petkova, A. T., Ishii, Y., Balbach, J. J., Antzutkin, O. N., Leapman, R. D., Delaglio, F., and Tycko, R. (2002) A structural model for Alzheimer's beta-amyloid fibrils based on experimental constraints from solid state NMR. *Proc. Natl. Acad. Sci. U.S.A.* **99,** 16742–16747 CrossRef Medline
10. Qiang, W., Yau, W. M., Lu, J. X., Collinge, J., and Tycko, R. (2017) Structural variation in amyloid-beta fibrils from Alzheimer's disease clinical subtypes. *Nature* **541,** 217–221 CrossRef Medline
11. Ahmed, M., Davis, J., Aucoin, D., Sato, T., Ahuja, S., Aimoto, S., Elliott, J. I., Van Nostrand, W. E., and Smith, S. O. (2010) Structural conversion of neurotoxic amyloid-beta(1–42) oligomers to fibrils. *Nat. Struct. Mol. Biol.* **17,** 561–567 CrossRef Medline
12. Yu, L., Edalji, R., Harlan, J. E., Holzman, T. F., Lopez, A. P., Labkovsky, B., Hillen, H., Barghorn, S., Ebert, U., Richardson, P. L., Miesbauer, L., Solomon, L., Bartley, D., Walter, K., Johnson, *et al.* (2009) Structural characterization of a soluble amyloid beta-peptide oligomer. *Biochemistry* **48,** 1870–1877 CrossRef Medline
13. Stroud, J. C., Liu, C., Teng, P. K., and Eisenberg, D. (2012) Toxic fibrillar oligomers of amyloid-beta have cross-beta structure. *Proc. Natl. Acad. Sci. U.S.A.* **109,** 7717–7722 CrossRef Medline
14. Fu, Z., Aucoin, D., Davis, J., Van Nostrand, W. E., and Smith, S. O. (2015) Mechanism of nucleated conformational conversion of Aβ42. *Biochemistry* **54,** 4197–4207 CrossRef Medline
15. Wisniewski, T., Ghiso, J., and Frangione, B. (1991) Peptides homologous to the amyloid protein of Alzheimer's disease containing a glutamine for glutamic acid substitution have accelerated amyloid fibril formation. *Biochem. Biophys. Res. Commun.* **179,** 1247–1254 CrossRef Medline
16. Bush, A. I., Pettingell, W. H., Multhaup, G., d Paradis, M., Vonsattel, J. P., Gusella, J. F., Beyreuther, K., Masters, C. L., and Tanzi, R. E. (1994) Rapid induction of Alzheimer A beta amyloid formation by zinc. *Science* **265,** 1464–1467 CrossRef Medline
17. Cherny, R. A., Atwood, C. S., Xilinas, M. E., Gray, D. N., Jones, W. D., McLean, C. A., Barnham, K. J., Volitakis, I., Fraser, F. W., Kim, Y., Huang, X., Goldstein, L. E., *et al.* (2001) Treatment with a copper-zinc chelator markedly and rapidly inhibits beta-amyloid accumulation in Alzheimer's disease transgenic mice. *Neuron* **30,** 665–676 CrossRef Medline
18. Yanagisawa, K., Odaka, A., Suzuki, N., and Ihara, Y. (1995) GM1 ganglioside-bound amyloid beta-protein (A beta): A possible form of preamyloid in Alzheimer's disease. *Nat. Med.* **1,** 1062–1066 CrossRef Medline
19. Harder, T., Scheiffele, P., Verkade, P., and Simons, K. (1998) Lipid domain structure of the plasma membrane revealed by patching of membrane components. *J. Cell Biol.* **141,** 929–942 CrossRef Medline
20. Merritt, E. A., Sarfaty, S., van den Akker, F., L'Hoir, C., Martial, J. A., and Hol, W. G. (1994) Crystal structure of cholera toxin B-pentamer bound to receptor GM1 pentasaccharide. *Protein Sci.* **3,** 166–175 Medline
21. Sonnino, S., Prinetti, A., Mauri, L., Chigorno, V., and Tettamanti, G. (2006) Dynamic and structural properties of sphingolipids as driving forces for the formation of membrane domains. *Chem. Rev.* **106,** 2111–2125 CrossRef Medline
22. Simons, K., and Vaz, W. L. (2004) Model systems, lipid rafts, and cell membranes. *Annu. Rev. Biophys. Biomol. Struct.* **33,** 269–295 CrossRef Medline
23. Yanagisawa, K. (2011) Pathological significance of ganglioside clusters in Alzheimer's disease. *J. Neurochem.* **116,** 806–812 CrossRef Medline
24. Sakono, M., and Zako, T. (2010) Amyloid oligomers: Formation and toxicity of Abeta oligomers. *FEBS J.* **277,** 1348–1358 CrossRef Medline
25. Yanagisawa, K. (2007) Role of gangliosides in Alzheimer's disease. *Biochim. Biophys. Acta* **1768,** 1943–1951 CrossRef Medline
26. Yanagisawa, K. (2015) GM1 ganglioside and Alzheimer's disease. *Glycoconj. J.* **32,** 87–91 CrossRef Medline
27. Yamamoto, N., Matsubara, E., Maeda, S., Minagawa, H., Takashima, A., Maruyama, W., Michikawa, M., and Yanagisawa, K. (2007) A ganglioside-induced toxic soluble Abeta assembly: Its enhanced formation from Abeta bearing the Arctic mutation. *J. Biol. Chem.* **282,** 2646–2655 CrossRef Medline
28. Evangelisti, E., Cascella, R., Becatti, M., Marrazza, G., Dobson, C. M., Chiti, F., Stefani, M., and Cecchi, C. (2016) Binding affinity of amyloid oligomers to cellular membranes is a generic indicator of cellular dysfunction in protein misfolding diseases. *Sci. Rep.* **6,** 32721 CrossRef Medline
29. Matsubara, T., Iijima, K., Yamamoto, N., Yanagisawa, K., and Sato, T. (2013) Density of GM1 in nanoclusters is a critical factor in the formation of a spherical assembly of amyloid beta-protein on synaptic plasma membranes. *Langmuir* **29,** 2258–2264 CrossRef Medline
30. Matsubara, T., Nishihara, M., Yasumori, H., Nakai, M., Yanagisawa, K., and Sato, T. (2017) Size and shape of amyloid fibrils induced by ganglioside nanoclusters: Role of sialyl oligosaccharide in fibril formation. *Langmuir* **33,** 13874–13881 CrossRef Medline
31. Oikawa, N., Matsubara, T., Fukuda, R., Yasumori, H., Hatsuta, H., Murayama, S., Sato, T., Suzuki, A., and Yanagisawa, K. (2015) Imbalance in fatty-acid-chain length of gangliosides triggers Alzheimer amyloid deposition in the precuneus. *PloS One* **10,** e0121356 CrossRef Medline
32. Matsuzaki, K., and Horikiri, C. (1999) Interactions of amyloid beta-peptide (1–40) with ganglioside-containing membranes. *Biochemistry* **38,** 4137–4142 CrossRef Medline
33. Fukunaga, S., Ueno, H., Yamaguchi, T., Yano, Y., Hoshino, M., and Matsuzaki, K. (2012) GM1 cluster mediates formation of toxic Abeta fibrils by providing hydrophobic environments. *Biochemistry* **51,** 8125–8131 CrossRef Medline
34. Utsumi, M., Yamaguchi, Y., Sasakawa, H., Yamamoto, N., Yanagisawa, K., and Kato, K. (2009) Up-and-down topological mode of amyloid beta-peptide lying on hydrophilic/hydrophobic interface of ganglioside clusters. *Glycoconj. J.* **26,** 999–1006 CrossRef Medline
35. Yagi-Utsumi, M., Kameda, T., Yamaguchi, Y., and Kato, K. (2010) NMR characterization of the interactions between lyso-GM1 aqueous micelles and amyloid beta. *FEBS Lett.* **584,** 831–836 CrossRef Medline
36. Yagi-Utsumi, M., and Kato, K. (2015) Structural and dynamic views of GM1 ganglioside. *Glycoconj. J.* **32,** 105–112 CrossRef Medline
37. Hu, Z., Wang, X., Wang, W., Zhang, Z., Gao, H., and Mao, Y. (2015) Raman spectroscopy for detecting supported planar lipid bilayers composed of ganglioside-GM1/sphingomyelin/cholesterol in the presence of amyloid-beta. *Phys. Chem. Chem. Phys.* **17,** 22711–22720 CrossRef Medline
38. Yamamoto, N., Matsubara, T., Sato, T., and Yanagisawa, K. (2008) Age-dependent high-density clustering of GM1 ganglioside at presynaptic neuritic terminals promotes amyloid beta-protein fibrillogenesis. *Biochim. Biophys. Acta* **1778,** 2717–2726 CrossRef Medline
39. Kakio, A., Nishimoto, S. I., Yanagisawa, K., Kozutsumi, Y., and Matsuzaki, K. (2001) Cholesterol-dependent formation of GM1 ganglioside-bound amyloid beta-protein, an endogenous seed for Alzheimer amyloid. *J. Biol. Chem.* **276,** 24985–24990 CrossRef Medline
40. Tycko, R. (2011) Solid-state NMR studies of amyloid fibril structure. *Annu. Rev. Phys. Chem.* **62,** 279–299 CrossRef Medline
41. Lu, J. X., Qiang, W., Yau, W. M., Schwieters, C. D., Meredith, S. C., and Tycko, R. (2013) Molecular structure of beta-amyloid fibrils in Alzheimer's disease brain tissue. *Cell* **154,** 1257–1268 CrossRef Medline
42. Hayashi, H., Kimura, N., Yamaguchi, H., Hasegawa, K., Yokoseki, T., Shibata, M., Yamamoto, N., Michikawa, M., Yoshikawa, Y., Terao, K., Matsuzaki, K., Lemere, C. A., Selkoe, D. J., Naiki, H., and Yanagisawa, K. (2004) A seed for Alzheimer amyloid in the brain. *J. Neurosci.* **24,** 4894–4902 CrossRef Medline
43. Gun, J., Iscovici, R., and Sagiv, J. (1984) On the formation and structure of self-assembling monolayers: II. A comparative study of Langmuir–Blodgett and adsorbed films using ellipsometry and IR reflection–absorption spectroscopy. *J. Colloid Interface Sci.* **101,** 201–213 CrossRef
44. Dreissig, I., Machill, S., Salzer, R., and Krafft, C. (2009) Quantification of brain lipids by FTIR spectroscopy and partial least squares regression. *Spectrochim Acta A Mol Biomol Spectrosc.* **71,** 2069–2075 CrossRef Medline
45. Moore, D. J., Rerek, M. E., and Mendelsohn, R. (1997) FTIR spectroscopy studies of the conformational order and phase behavior of ceramides. *J. Phys. Chem. B* **101,** 8933–8940 CrossRef
46. Byler, D. M., and Susi, H. (1986) Examination of the secondary structure of proteins by deconvolved FTIR spectra. *Biopolymers* **25,** 469–487 CrossRef Medline
47. Bandekar, J. (1992) Amide modes and protein conformation. *Biochim. Biophys. Acta* **1120,** 123–143 CrossRef Medline

48. Surewicz, W. K., Mantsch, H. H., and Chapman, D. (1993) Determination of protein secondary structure by Fourier transform infrared spectroscopy: A critical assessment. *Biochemistry* **32,** 389–394 CrossRef Medline
49. Kong, J., and Yu, S. (2007) Fourier transform infrared spectroscopic analysis of protein secondary structures. *Acta Biochim. Biophys. Sin.* (*Shanghai*) **39,** 549–559 CrossRef Medline
50. Pelton, J. T., and McLean, L. R. (2000) Spectroscopic methods for analysis of protein secondary structure. *Anal. Biochem.* **277,** 167–176 CrossRef Medline
51. Yamada, N., Ariga, K., Naito, M., Matsubara, K., and Koyama, E. (1998) Regulation of β-sheet structures within amyloid-like β-sheet assemblage from tripeptide derivatives. *J. Am. Chem. Soc.* **120,** 12192–12199 CrossRef
52. Hoshino, T., Mahmood, M. I., Mori, K., and Matsuzaki, K. (2013) Binding and aggregation mechanism of amyloid beta-peptides onto the GM1 ganglioside-containing lipid membrane. *J. Phys. Chem. B* **117,** 8085–8094 CrossRef Medline
53. Shimoaka, T., Rikiyama, K., Katsumoto, Y., and Hasegawa, T. (2013) Infrared spectroscopic study of stereo-controlled poly(*N*-isopropylacrylamide) with an extended chain conformation induced by adsorption on a gold surface. *Anal. Bioanal. Chem.* **405,** 9411–9418 CrossRef Medline
54. Susi, H., and Byler, D. M. (1983) Protein structure by Fourier transform infrared spectroscopy: Second derivative spectra. *Biochem. Biophys. Res. Commun.* **115,** 391–397 CrossRef Medline
55. Dong, A., Huang, P., and Caughey, W. S. (1990) Protein secondary structures in water from second-derivative amide I infrared spectra. *Biochemistry* **29,** 3303–3308 CrossRef Medline